

Oriental phase transition of microtubules in 3D using mean-field theory

Cameron Gibson^{1,*}, Tamsin A. Spelman¹, and Henrik Jönsson^{1,2,3†}

¹ *Sainsbury Laboratory, University of Cambridge, Cambridge, UK.*

² *Department of Applied Mathematics and Theoretical Physics, University of Cambridge, Cambridge, UK.*

³ *Computational Biology and Biological Physics Group,
Department of Astronomy and Theoretical Physics, Lund University, Lund, Sweden.*

(Dated: February 22, 2022)

Microtubules are active fibers which form one part of a plant cell cytoskeleton, and have been observed experimentally to undergo spontaneous self-alignment. Here, we formulate a 3D mean-field theory model in order to analyze the orientational phase transition of microtubules interacting within 3D space. Having identified a control parameter, dependent on microtubule properties, we predict the value of the control parameter for which a phase transition is possible. We then use computer simulations to show that there is a change in orientational order at the predicted control parameter value. We also show that simulations support the mean-field model prediction that the presence of zippering does not affect this critical control parameter value.

I. INTRODUCTION

Microtubules are polymers of tubulin that form an active fiber network in all eukaryotic cells [1]. In plant cells, together with actin microfilaments, they form the cytoskeleton [2, 3]. The cytoskeleton is vital in plant cells for cell division, expansion, and morphogenesis [4–6]. Each microtubule has a plus end and a minus end which both either grow or shrink via the assembly and disassembly of tubulin [7]. For our model, we assume that the minus end is static since it changes at a much slower rate than the plus end [8].

Microtubule networks exhibit similarities with the condensed matter system of nematic liquid crystals [9, 10] as they can both be viewed as systems of many hard interacting rods. Furthermore, high levels of spontaneous alignment have been observed experimentally in microtubule systems which are qualitatively similar to phase transitions in nematic liquid crystals [11]. Various models have been proposed to analyze cytoskeletal dynamics [12–15]. A useful continuum theory approach is mean-field theory [16], which is often used to analyze condensed matter systems [17] and to analyze microtubule dynamics [18–22].

In [21], a 2D mean-field theory model for microtubule dynamics was analyzed, but excluding induced catastrophe dynamics, which refers to a growing microtubule spontaneously switching to shrinking in response to collision with another microtubule. These induced catastrophe dynamics were included in the model of [22], where they formulated a 2D mean-field theory of microtubules and proved the existence of a phase transition under certain assumptions. In this paper, we extend the 2D model in [22] to 3D in a novel way, highlighting the differences and similarities between the two cases.

This paper is organized as follows. In Sec. II, we set up the 3D equations governing the system and solve them in the isotropic case. We also describe the computational model we use to simulate microtubule dynamics. In Sec. III A, we compare the 2D mean-field model in [22] with our 3D model, then determine constraints on our system that allow for a phase transition in 3D in Sec. III B. In Sec. III C, we compare the predictions of the mean-field theory model with results of the computational simulations.

II. MODEL

Here, we outline our model. Note that we will use spherical polar coordinates to describe directions in 3D space, denoted by (θ, ϕ) and use the convention that θ and ϕ are the polar and azimuthal angles respectively. When comparing to the 2D case, we will similarly use the 2D polar coordinate θ to describe direction in 2D space.

A. Assumptions

In this subsection, we state the key assumptions that we make about our system of microtubules.

Firstly, we assume that microtubules nucleate everywhere in 3D space at a constant rate $\frac{r_n}{4\pi}$, are static at the minus end, and are either growing or shrinking at the plus end with speed v^+ or v^- respectively. The plus end changes from shrinking to growing via spontaneous rescue with rate r_r and changes from growing to shrinking via spontaneous catastrophe with rate r_c .

We assume that unhindered microtubules grow in a straight line, with some probability of changing direction when two microtubules collide in a process called zippering. The microtubules grow (and shrink) in segments, with joints allowing each segment to be oriented in a different direction. Specifically, when a growing seg-

* Cameron.Gibson@slcu.cam.ac.uk

† Henrik.Jonsson@slcu.cam.ac.uk

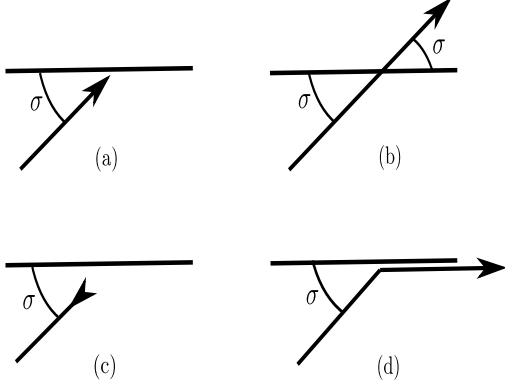


FIG. 1: (a) Collision: a growing microtubule segment collides with another segment at collision angle σ . (b) Crossover: the segment continues to grow unhindered. (c) Induced catastrophe: the segment switches from growing to shrinking. (d) Zippering: the segment starts to grow parallel to the segment it collides with.

ment collides with a second segment, either there is an induced catastrophe (it starts shrinking), crossover (it keeps growing unhindered) or zippering (it starts growing parallel to the second segment) with respective probabilities $P_c(\sigma)$, $P_x(\sigma)$ and $P_z(\sigma)$ all written as functions of the collision angle σ . These events are illustrated in Figure. 1.

B. Master Equations

In this subsection, we determine the differential equations governing the physical system of interacting microtubules. For further details, see [22] where the similar 2D equations are derived.

We assume that the density of microtubules is large enough so that we can work with a continuum theory, allowing us to define a macroscopic description of the system. This encourages us to define $m_i^{+/-/0}(l, \theta, \phi, t)$ as the density of microtubule segments in direction (θ, ϕ) of length l at time t with $+/-/0$ indicating a growing/shrinking/inactive segment respectively and i indexing the segments (letting $i = 1$ index the segment that has nucleated).

Then, the master equations governing the evolution of our system can be expressed in terms of flux terms de-

noted Φ_{event} .

$$\begin{aligned} \partial_t m_i^+(l_i, \theta_i, \phi_i, t) &= \Phi_{growth} + \Phi_{rescue} - \Phi_{spontcat} \\ &\quad - \Phi_{inducedcat} - \Phi_{zipper}, \\ \partial_t m_i^-(l_i, \theta_i, \phi_i, t) &= \Phi_{shrinkage} - \Phi_{rescue} + \Phi_{spontcat} \\ &\quad + \Phi_{inducedcat} + \Phi_{reactivation}, \\ \partial_t m_i^0(l_i, \theta_i, \phi_i, t) &= \Phi_{zipper} - \Phi_{reactivation}. \end{aligned} \quad (1)$$

There is a flux term

$$\Phi_{growth} \equiv -v^+ \partial_{l_i} m_i^+(l_i, \theta_i, \phi_i, t), \quad (2)$$

derived from $-v^+ \partial_{l_i} m_i^+ = \frac{\partial l_i}{\partial t} \partial_{l_i} m_i^+ = \partial_t m_i^+$ and a flux term

$$\Phi_{shrinkage} \equiv v^- \partial_{l_i} m_i^-(l_i, \theta_i, \phi_i, t), \quad (3)$$

derived from $v^- \partial_{l_i} m_i^- = \frac{\partial l_i}{\partial t} \partial_{l_i} m_i^- = \partial_t m_i^-$. The flux terms

$$\Phi_{rescue} \equiv r_r m_i^-(l_i, \theta_i, \phi_i, t), \Phi_{spontcat} \equiv r_c m_i^+(l_i, \theta_i, \phi_i, t) \quad (4)$$

arise from spontaneous rescue and spontaneous catastrophe respectively.

There is also a flux term

$$\begin{aligned} \Phi_{reactivation} &\equiv v^- \int d\theta_{i+1} \int d\phi_{i+1} \sin(\theta_{i+1}) \\ &\quad \times m_{i+1}^-(l_{i+1} = 0, \theta_{i+1}, \phi_{i+1}, t) p_{unzip}(\theta_i, \phi_i, l_i | \theta_{i+1}, \phi_{i+1}, t) \end{aligned} \quad (5)$$

where $p_{unzip}(\theta_i, \phi_i, l_i | \theta_{i+1}, \phi_{i+1}, t)$ is the probability that the $(i+1)^{th}$ segment shrinks from the direction $(\theta_{i+1}, \phi_{i+1})$ to length zero at time t and reactivates the i^{th} segment of length l_i in direction (θ_i, ϕ_i) . Detailed arguments as to why p_{unzip} is already determined by our previous assumptions are given in [22], which naturally extend from 2D to 3D.

Let

$$\begin{aligned} k(\theta, \phi, t) &\equiv \sum_i \int dl_i l_i [m_i^+(l_i, \theta, \phi, t) + m_i^-(l_i, \theta, \phi, t) \\ &\quad + m_i^0(l_i, \theta, \phi, t)] \end{aligned} \quad (6)$$

be the length density of microtubules pointing in direction (θ, ϕ) . We can then consider the induced catastrophe flux term

$$\begin{aligned} \Phi_{inducedcat} &\equiv v^+ m_i^+(l_i, \theta_i, \phi_i, t) \int d\theta' \int d\phi' \sin(\theta') \\ &\quad \times c(\theta_i, \theta', \phi_i - \phi') k(\theta', \phi', t), \end{aligned} \quad (7)$$

where, in 3D, we define

$$c(\theta, \theta', \phi - \phi') \equiv |\sin(\sigma)| P_c(\sigma(\theta, \theta', \phi - \phi')), \quad (8)$$

also defining

$$\sigma = \arccos(\sin(\theta) \sin(\theta') \cos(\phi - \phi') + \cos(\theta) \cos(\theta')). \quad (9)$$

as the angle between the two directions (θ, ϕ) and (θ', ϕ') . The $|\sin(\sigma)|$ factor in Eq. 8 compensates for the fact that the probability of collision depends on the angle between interacting segments. For example, perpendicular interacting segments will collide and parallel interacting segments will not collide. Φ_{zipper} is defined similarly as $\Phi_{inducedcat}$ is in Eq. 7 but with c replaced by z . These collision events are represented in Figure. 1.

C. Control Parameter

An important parameter in our system is $g = \frac{r_r}{v^-} - \frac{r_c}{v^+}$ [21, 22]. Physically, g corresponds to the non-interacting behavior of the microtubules. $g \rightarrow -\infty$ corresponds to an overwhelmingly catastrophic and trivially isotropic system, whilst $g \rightarrow \infty$ corresponds to an overwhelmingly growing and trivially anisotropic system. Following our earlier analogy of a phase transition in a liquid crystal system, our control parameter g is analogous to temperature in liquid crystals. Therefore, we expect there to be an orientational phase transition as we increase g from negative infinity. Importantly, we note that the only physically realizable values of g are negative, since positive g corresponds to unbounded growth.

D. Steady State System

In this subsection, we write down the equations describing the steady state system that arise from the master equations Eq. 1. A complete derivation of similar steady state equations for the 2D system is given in [22].

We define $l(\theta, \phi)$ to be the average segment length in the direction (θ, ϕ) :

$$\frac{1}{l(\theta, \phi)} = -g + \int d\theta' \int d\phi' \sin(\theta') [c(\theta, \theta', \phi - \phi') + z(\theta, \theta', \phi - \phi')] k(\theta', \phi'). \quad (10)$$

We define $Q(\theta, \phi)$ as the ratio of inactive (static at both ends) to active (both growing and shrinking) segments in the direction (θ, ϕ) :

$$Q(\theta, \phi) = \frac{m^0(\theta, \phi)}{m^+(\theta, \phi) + m^-(\theta, \phi)}. \quad (11)$$

We define $t(\theta, \phi)$ to be the density of active segments in the direction (θ, ϕ) :

$$t(\theta, \phi) = \left(1 + \frac{v^+}{v^-}\right) l(\theta, \phi) \sum_{i=1}^{\infty} m_i^+(\theta, \phi). \quad (12)$$

For convenience, we define dimensionless quantities by first defining a variable l_0 with dimensions of length.

$$l_0 = \left[\left(\frac{1}{v^+} + \frac{1}{v^-} \right) \frac{r_n}{4\pi} \right]^{-\frac{1}{4}}. \quad (13)$$

Our dimensionless quantities are then $G = gl_0$, $L = ll_0^{-1}$, $K = kl_0^2$ and $T = tl_0^3$.

Even though it has been made dimensionless, G is still the control parameter of our system:

$$G = \left[\frac{4\pi v^+ v^-}{r_n(v^+ + v^-)} \right]^{\frac{1}{4}} \left(\frac{r_r}{v^-} - \frac{r_c}{v^+} \right). \quad (14)$$

We also summarize expressions like Eq. 7 by defining the linear operator

$$F[h](\theta, \phi) = \int_0^\pi d\theta' \int_0^{2\pi} d\phi' \sin(\theta') f(\theta, \theta', \phi - \phi') h(\theta', \phi'), \quad (15)$$

for $F \in [C, Z]$.

The steady state 3D equations are then the following:

$$\begin{aligned} \frac{1}{L(\theta, \phi)} &= -G + C[K](\theta, \phi) + Z[K](\theta, \phi), \\ K(\theta, \phi) &= L(\theta, \phi)(1 + Q(\theta, \phi))T(\theta, \phi), \\ Q(\theta, \phi) &= Z[LK(1 + Q)](\theta, \phi), \\ T(\theta, \phi) &= L(\theta, \phi) + L(\theta, \phi)K(\theta, \phi)Z[T](\theta, \phi). \end{aligned} \quad (16)$$

E. Isotropic Solution

In this subsection, we consider the isotropic case of the steady state 3D equations Eq. 16, then solve this system.

The spherical harmonics [23, 24] are a complete set of orthogonal functions $Y_\ell^m : S^2 \rightarrow \mathbb{R}$ with two indices (ℓ and m) that can be defined in the following way. Note that we have chosen them to be real-valued functions as follows:

$$Y_\ell^m(\theta, \phi) = \begin{cases} (-1)^m \sqrt{\frac{2\ell+1}{2\pi} \frac{(\ell-|m|)!}{(\ell+|m|)!}} P_\ell^{|m|}(\cos(\theta)) \sin(|m|\phi) & m < 0, \\ \sqrt{\frac{2\ell+1}{4\pi}} P_\ell^m(\cos(\theta)) & m = 0, \\ (-1)^m \sqrt{\frac{2\ell+1}{2\pi} \frac{(\ell-m)!}{(\ell+m)!}} P_\ell^m(\cos(\theta)) \cos(m\phi) & m > 0. \end{cases} \quad (17)$$

Here, P_ℓ^m are the associated Legendre polynomials, defined in terms of the standard Legendre polynomials P_ℓ :

$$P_\ell^m(\cos \theta) = (-1)^m (\sin \theta)^m \frac{d^m}{d(\cos \theta)^m} (P_\ell(\cos \theta)). \quad (18)$$

$$P_\ell(x) = \frac{1}{2^\ell \ell!} \frac{d^\ell}{dx^\ell} (x^2 - 1)^\ell. \quad (19)$$

The spherical harmonics defined by Eq. 17 provide an orthonormal basis of eigenfunctions of the linear operator defined in Eq. 15. To prove this, we first make a change of variables in Eq. 15 via $f(\sigma) \equiv \mathfrak{F}(\cos(\sigma))$ with $f \in [c, z]$ and $\mathfrak{F} \in [\mathfrak{C}, \mathfrak{Z}]$ respectively, and with σ defined by Eq. 9. We then make a Legendre expansion

$$\mathfrak{F}(\cos(\sigma)) = \sum_{\ell=0}^{\infty} \mathfrak{F}_{\ell} P_{\ell}(\cos(\sigma)) \quad (20)$$

$$\text{where } \mathfrak{F}_{\ell} = \frac{2\ell+1}{2} \int_{-1}^1 \mathfrak{F}(x) P_{\ell}(x) dx. \quad (21)$$

Then, using the spherical harmonic addition theorem [23, 24]

$$P_{\ell}(\cos(\sigma)) = \frac{4\pi}{2\ell+1} \sum_{m=-\ell}^{\ell} Y_{\ell}^m(\theta, \phi) Y_{\ell}^{m*}(\theta', \phi'), \quad (22)$$

we rewrite Eq. 20 and substitute this into Eq. 15. Finally, we simplify with the standard orthogonality condition of spherical harmonics

$$\int_0^{\pi} d\theta' \int_0^{2\pi} d\phi' \sin(\theta') Y_{\ell}^m(\theta', \phi') Y_{\ell'}^{m'}(\theta', \phi') = \delta_{\ell\ell'} \delta^{mm'}, \quad (23)$$

giving us the eigenvalue equation

$$F[Y_{\ell}^m(\theta, \phi)] = \frac{4\pi\mathfrak{F}_{\ell}}{2\ell+1} Y_{\ell}^m(\theta, \phi). \quad (24)$$

We can now use Eq. 24 with $\ell = m = 0$ to obtain $F[1] = 4\pi\mathfrak{F}_0$. In the isotropic (and stationary) state of the system, all angular dependence drops out of our variables, which we denote with an overbar over the previously defined variables, and our system of equations in Eqs. 16 becomes

$$\begin{aligned} \frac{1}{\bar{L}} &= -G + (4\pi\mathfrak{C}_0 + 4\pi\mathfrak{Z}_0)\bar{K} \\ \bar{K} &= \bar{L}(1 + \bar{Q})\bar{T} \\ \bar{Q} &= 4\pi\mathfrak{Z}_0\bar{L}\bar{K}(1 + \bar{Q}) \\ \bar{T} &= \bar{L} + 4\pi\mathfrak{Z}_0\bar{L}\bar{K}\bar{T}. \end{aligned} \quad (25)$$

Eqs. 25 together imply the following relation:

$$\bar{K}(4\pi\mathfrak{C}_0\bar{K} - G)^2 = 1. \quad (26)$$

This relation implies that, given one of \bar{K} and G , there is a unique solution for the other if $\mathfrak{C}_0 > 0$ (since we must have a non-negative density \bar{K} and $G < 0$ for a physically realizable system). We will consider a positive value of \mathfrak{C}_0 that reasonably matches experiment in Sec. III B.

F. Simulation

In order to compare the predictions from our 3D mean-field theory model to 3D simulations, we use a discretized

model of microtubule dynamics, extending the 3D microtubule simulation Tubulaton developed for [25, 26]. This models each microtubule individually as end-to-end unit vectors. They can grow and shrink, incorporating microtubule interaction dynamics such as zippering and induced catastrophe as well as individual microtubule dynamics such as nucleation and spontaneous catastrophe. An external membrane is prescribed within which microtubules remain. When microtubules interact with the boundary, they either undergo catastrophe or turning along the boundary depending on interaction angle.

Our extension to the simulation Tubulaton allows microtubules to nucleate isotropically within a 3D spherical space in order to match our mean-field theory assumptions. The radius of the nucleation region is prescribed and nucleation will occur in a region of this size centered on the center of the external membrane. To reflect isotropic nucleation everywhere, we fix three radii of increasing magnitude: one below which we analyze the data to calculate the anisotropy level of microtubules, one below which microtubules can nucleate, and one which forms the boundary of the system. Importantly, we can vary $P_c(\sigma)$ and $P_z(\sigma)$ as well as r_c and r_n . We do not include the effects of spontaneous rescue in our model since our interest is in negative G (as defined in Eq. 14) and varying r_c can give us the full range of negative values of G .

G. Order Parameter

Following our earlier comparisons to nematic liquid crystals, we use the standard nematic order parameter [9, 10, 27] to quantify the alignment in our system. In d dimensions, this is a unique tensor up to an overall factor, which we normalize by setting to unity in the completely anisotropic state:

$$S_{ab} = \left\langle \frac{d}{d-1} n_a n_b - \frac{1}{d-1} \delta_{ab} \right\rangle, \quad (27)$$

where $\langle \rangle$ denotes taking an average over all microtubules which each have a unit vector n_a describing their direction. In 3D, we therefore have the 3x3 matrix

$$S = \frac{\int_0^{\pi} d\theta \int_0^{2\pi} d\phi \sin(\theta) K(\theta, \phi) \left(\frac{3}{2} n \otimes n - \frac{1}{2} \mathcal{I} \right)}{\int_0^{\pi} d\theta \int_0^{2\pi} d\phi \sin(\theta) K(\theta, \phi)}. \quad (28)$$

S has three eigenvalues: these are all zero if and only if the system is in its completely isotropic state. Although there are subtleties involved in extracting a scalar order parameter from Eq. 28, we take the maximum absolute value of the eigenvalues of S increasing as an effective indicator of whether our system changes from an isotropic state to an anisotropic state.

Note that all graphing in this paper in Sec. III is done using MATLAB R2021a.

III. RESULTS

A. Comparison to 2D Model

Here, we compare our 3D model to the 2D model developed in [22].

Importantly, the original control parameter $g = \frac{r_c}{v^-} - \frac{r_r}{v^+}$ remains the same. However, there are expected differences in the definition of l_0 , defined in Eq. 13, which is chosen to have dimensions of length. There are also differences in the factors of l_0 involved in nondimensionalizing g and other variables describing the system.

There is a difference in how the induced catastrophe flux term in Eq. 7 is defined, with the factor $|\sin(\sigma)|$ adjusting for varying collision probability. We have the collision angle defined in 3D as $\sigma = \arccos(\sin(\theta)\sin(\theta')\cos(\phi - \phi') + \cos(\theta)\cos(\theta'))$ instead of $\sigma = \theta$ in 2D.

The difference in the catastrophe flux term in 3D leads to significant differences from the 2D model in Sec. II E. Immediately, the linear operator defined in Eq. 15 is different. In 3D, the spherical harmonics provide an orthonormal basis of eigenfunctions, instead of Fourier modes in 2D. Viewing the spherical harmonics $Y_\ell^m : S^2 \rightarrow \mathbb{R}$ as a higher dimensional analog of $S^1 \rightarrow \mathbb{R}$ Fourier modes [28], this higher dimensional generalization is perhaps to be expected. As a result of this difference, Eq. 25 and Eq. 26 both involve Legendre coefficients in 3D instead of Fourier coefficients in 2D.

B. Perturbative Analysis

In this subsection, we consider the constraints we must place on our system if a physically realizable change in microtubule alignment can occur.

In order to reach an ordered state from the isotropic state (i.e. undergo a phase transition), the system must first undergo a small perturbation away from the isotropic configuration. Motivated by this, we define small perturbations $\lambda, \kappa, \chi, \tau$ to the variables in our system via

$$\begin{aligned} L &= \bar{L}(1 + \lambda), & K &= \bar{K}(1 + \kappa), \\ Q &= \bar{Q}(1 + \chi), & T &= \bar{T}(1 + \tau). \end{aligned} \quad (29)$$

Following the 2D case in [22], we require that Eqs. 25 hold to first order in $\lambda, \kappa, \chi, \tau$ then put each side of the second of these first order equations as the functional argument of $Z[\]$. Then, after a linear rearrangement of the resulting equations, we get the eigenvalue equation

$$(1 - 4\pi\mathfrak{z}_0\bar{N})\kappa = -2\bar{N}C[\kappa]. \quad (30)$$

where $\bar{N} = \bar{L}\bar{K}$. Recognizing this as a special case of Eq. 24 again gives us the spherical harmonics defined in Eq. 17 as an orthonormal basis of eigenfunctions for this eigenvalue equation.

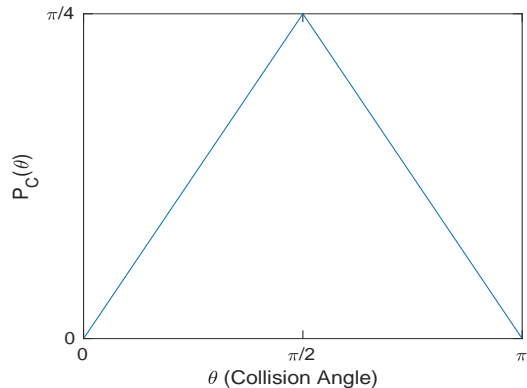


FIG. 2: Probability of induced catastrophe as a function of collision angle between two interacting microtubules. This is chosen to approximately match experimental results [29].

Since the eigenvalues in Eq. 24 only depend on the lower index ℓ of the spherical harmonics, each ℓ gives a value of \bar{N} for which there is a potential phase transition. We denote these as

$$\bar{N}_\ell^* = \left(4\pi\mathfrak{z}_0 - \frac{8\pi}{2\ell + 1}\mathfrak{C}_\ell\right)^{-1} \quad (31)$$

Eq. 26 then implies that these values of \bar{N} correspond to values of G (by extension also indexed by ℓ), which we write as

$$G_\ell^* = \left[1 + \frac{(2\ell + 1)\mathfrak{C}_0}{2\mathfrak{C}_\ell}\right] \left[-\frac{8\pi\mathfrak{C}_\ell}{2\ell + 1}\right]^{\frac{1}{3}}. \quad (32)$$

As in the 2D case, our model predicts that the location of a possible phase transition depends on P_c and not on P_z , since there is no dependence on \mathfrak{z}_ℓ in Eq. 32.

With the aim of reasonably matching experimental data [29], we choose $P_c(\sigma)$ to be two concatenated linear functions through the three points $(0, 0)$, $(\frac{\pi}{2}, \frac{\pi}{4})$, and $(\pi, 0)$. This is plotted in Figure. 2. We can then numerically calculate

$$\mathfrak{C}_\ell = \frac{2\ell + 1}{2} \int_0^\pi \sin^2(y) P_c(y) P_\ell(\cos(y)) dy, \quad (33)$$

an expression obtained from Eq. 21 through the change of variables $x \equiv \cos(y)$. Noting that \mathfrak{C}_ℓ vanishes for odd ℓ since $P_\ell(\cos(y))$ and therefore the integrand are odd functions about $y = \frac{\pi}{2}$, the values of \mathfrak{C}_ℓ are plotted numerically for $\ell = 0, 2, \dots, 200$ in Figure. 3. The corresponding values of G_ℓ^* are plotted in Figure. 4 using Eq. 32. As discussed in Sec. II C, only negative values of G correspond to physically realizable solutions with bounded growth, so it is promising that all plotted values of G_ℓ^* are negative. We now must identify which G_ℓ^* correspond to a physical perturbation of the system.

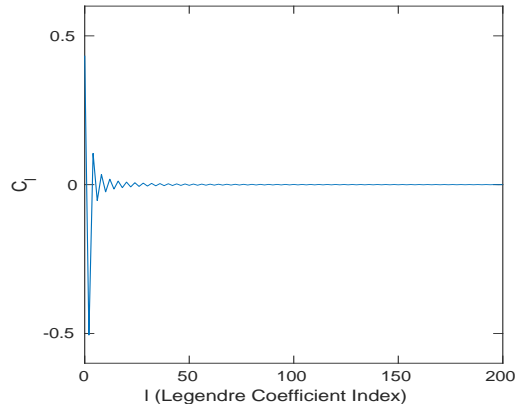


FIG. 3: The Legendre coefficients \mathfrak{C}_ℓ are plotted for $\ell = 0, 2, \dots, 200$ using Eq. 33.

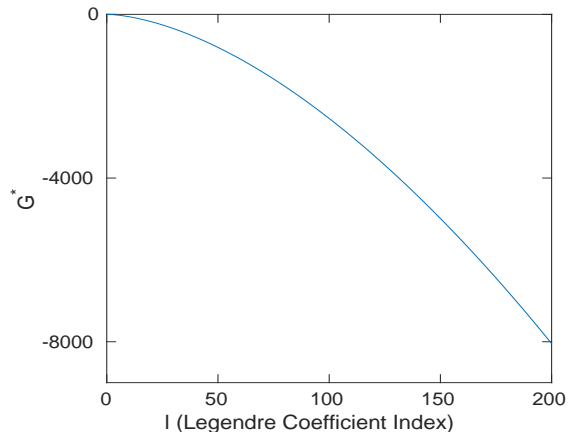
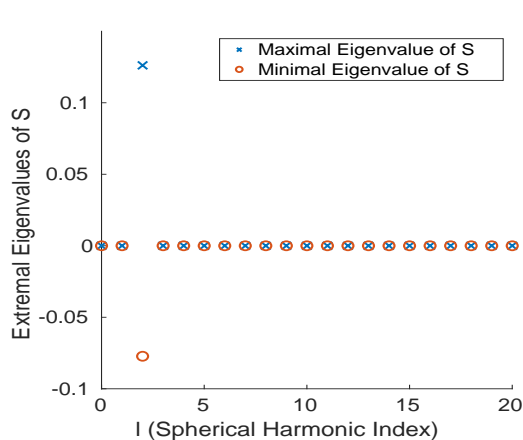
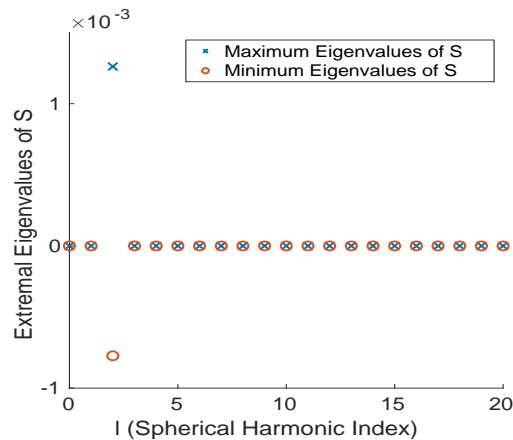


FIG. 4: The control parameter values that have the potential to give rise to a phase transition G_l^* are plotted for $l = 0, 2, \dots, 200$.



(a)



(b)

FIG. 5: Maximum and minimum eigenvalues of the 3D order parameter S are plotted against the spherical harmonic index ℓ of the perturbation κ .

(a) Results for κ taken to be spherical harmonics, normalized as in Eq. 17.

(b) Similar results with spherical harmonic perturbations divided by 100.

Without further analysis, we might conclude that every G_ℓ^* could correspond to physically realizable phase transitions. However, we need to consider whether the order of the system can actually be changed by the perturbations we are considering.

To evaluate whether the spherical harmonic perturbations $\kappa = Y_\ell^m$ actually change the order of the system, for each value of ℓ we take κ to be each of the corresponding $2\ell+1$ spherical harmonics (here, real and normalized) then calculate the extremal eigenvalues of the 3D order parameter S . The reasoning for this follows the discussion in Sec. II G. This is plotted in Figure. 5a for $\ell \leq 20$,

which singles out the $\ell = 2$ perturbations (the eigenvalues of S can be numerically bounded to be negligible) as the only ones which can affect the order of the system.

If all perturbations gave rise to this change in order, then a negligible change in some value of \mathfrak{C}_ℓ could drastically change the set of values of G_l^* whilst negligibly changing $P_c(\sigma)$. However, we have just shown that we should focus on \mathfrak{C}_2 and forget about the higher Legendre modes.

Since Eq. 29 is only valid when the perturbation κ is small, we repeat Figure. 5a after dividing each spherical harmonic perturbation by 1,000 to obtain Figure. 5b. We can see that we still get the same behavior that singles

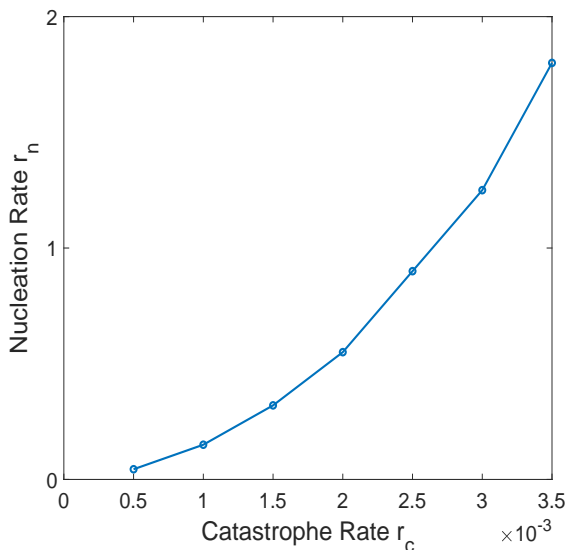


FIG. 6: Seven combinations of r_c and r_n for which the steady state number of microtubule segments (averaged over 50 simulations for each parameter set) whose data analyzed is between 95,000 and 105,000.

out $\ell = 2$ (although as we might expect, the change in order parameter is smaller for a smaller perturbation).

Therefore, we obtain $G^* \equiv G_2^* = -1.56$ (3sf) from Eq. 32 as our prediction of the control parameter value for which a phase transition is possible. We also predict that, for this value of G , when the density of microtubules $K(\theta, \phi)$ is perturbed slightly from its isotropic value by an $\ell = 2$ spherical harmonic, we expect anisotropy to enter the system.

C. Comparison to Simulation

We now validate our predictions against results from the detailed computational model of microtubule dynamics discussed in Sec. II F. We will increase G and show that the system undergoes a transition from disorder to order then make a comparison with the mean-field predicted value G^* . Furthermore, we validate that the value of G for which the system starts to align does not depend on zippering, which we expect as a result of Eq. 32.

To increase G , we alter both r_c and r_n on which G depends through Eq. 14. To ensure a change in isotropy is genuinely the result of changing the dynamics of our system and not a superficial result of changing the steady state density of microtubule segments, we keep the average number steady state number of microtubule segments (in the volume within which we perform our anisotropy calculation) within a fixed range. We choose this range to be 95,000 – 105,000 microtubule segments over 50 simulations for each parameter set. The path through the parameter sets (r_n, r_c) to obtain these similar steady

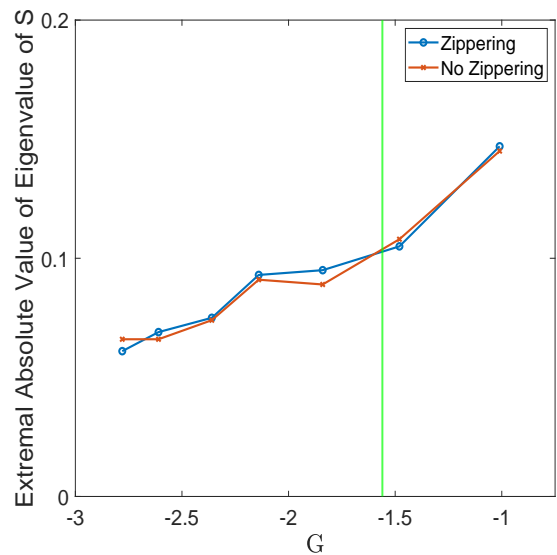


FIG. 7: Average extremal absolute eigenvalue of the order parameter S against control parameter G . The mean-field predicted value $G = -1.56$ (3sf) corresponding to a potential phase transition is represented by the green line.

states is plotted in Figure. 6. Outside the range plotted, it was not possible for the same steady state number of microtubule segments to be reached within simulations due to the number either blowing up or going to zero.

The values in Figure. 6 are close to a quadratic curve. Eq. 26 implies that in the isotropic state with constant microtubule density \bar{K} , G is constant. In this context, constant G corresponds to the relationship $r_n \propto r_c^4$. This could explain the convexity of Figure. 6, despite not matching the power law. Doubling r_n over 50 simulations provided an approximately doubled number of microtubule segments (i.e. in the range 190,000 – 210,000), suggesting that this relationship between r_n and r_c persists for higher microtubule segment densities.

In Figure. 7, we then use these values of r_c and r_n (note that we set v^+ equal to v^- in the simulations) to plot G against the maximal absolute value of the eigenvalues of the order parameter S . We plot this for two different zippering probability functions. In the first case, we approximately match experimental data [29] by choosing $P_z(\sigma) = 1 - P_c(\sigma) \forall \sigma \leq 0.7$ and $\sigma \geq \pi - 0.7 \leq$. In the second case, we remove zippering completely to see if this changes the computationally derived prediction of G^* .

The results of these simulations verifies two predictions from our mean-field theory model. Firstly, changing $P_z(\sigma)$ seems to have no effect on the orientational dynamics of the system as seen in Figure. 7. Secondly, we can see that our mean-field theory prediction $G^* = -1.56$ corresponding to a system switching from isotropy to anisotropy approximately matches the results of the simulations plotted in Figure. 7.

IV. DISCUSSION AND OUTLOOK

In this paper, we have developed a 3D mean-field theory model for an interacting system of microtubules. Having taken the induced catastrophe probability function $P_c(\sigma)$ to approximate experimental data, we determined numerically that there only exists one control parameter value $G^* = -1.56$ (3sf) for which a phase transition can occur. Furthermore, the mean-field theory model predicts that G^* only depends on $P_c(\sigma)$, not the zippering probability function $P_z(\sigma)$. Motivated by these predictions from the mean-field model, we utilized computer simulations to display the control parameter value for which order enters the systems. This approximately matched the predicted value of G^* . These simulations also verified the prediction that zippering does not affect the value of G^* , since the simulations resulted in similar behavior, regardless of whether zippering was present or not.

There are three clear ways in which this model could be

further developed. Firstly, it is unclear how the effects of severing [30] (where microtubule-severing enzymes break microtubules into smaller segments) could be introduced within the framework of mean-field theory or otherwise. Secondly, although a negative G gives bounded growth, introducing a hard boundary would be useful, especially in the context of considering different cell geometries. Thirdly, analytically solving the steady state equations Eqs. 16 (if possible), or making progress in considering general solutions, would hopefully contribute to a greater understanding of a phase transition taking place.

Acknowledgments All three authors acknowledge support from the Gatsby Charitable Foundation (GAT3395/PR4B) and additionally T.A.S and H.J acknowledge support from the Human Frontier Science Program Organization (Grant RGP0009/2018).

Data availability The 3D microtubule simulations were run using Tubulaton.

(<https://gitlab.com/sluc/teamHJ/tubulaton>).

-
- [1] Richard Wade. On and around microtubules: An overview. *Molecular biotechnology*, 43:177–91, 07 2009.
 - [2] R. H. Goddard, S. M. Wick, C. D. Silflow, and D. P. Snustad. Microtubule Components of the Plant Cell Cytoskeleton. *Plant Physiology*, 104(1):1–6, 01 1994.
 - [3] Daniel A. Fletcher and R. Dyché Mullins. Cell mechanics and the cytoskeleton. *Nature*, 463:485–492, 2010.
 - [4] Carolyn G. Rasmussen, Amanda J. Wright, and Sabine Müller. The role of the cytoskeleton and associated proteins in determination of the plant cell division plane. *The Plant Journal*, 75(2):258–269, 2013.
 - [5] Logan Bashline, Lei Lei, Shundai Li, and Ying Gu. Cell wall, cytoskeleton, and cell expansion in higher plants. *Molecular Plant*, 7(4):586–600, 2014.
 - [6] Whitney E. Hable, Sherryl R. Bisgrove, and Darryl L. Kropf. To Shape a Plant—The Cytoskeleton in Plant Morphogenesis. *The Plant Cell*, 10(11):1772–1774, 11 1998.
 - [7] Gary J. Brouhard. Dynamic instability 30 years later: complexities in microtubule growth and catastrophe. *Molecular Biology of the Cell*, 26(7):1207–1210, 2015. PMID: 25823928.
 - [8] Anna Akhmanova and Michel O. Steinmetz. Microtubule minus-end regulation at a glance. *Journal of Cell Science*, 132(11), 06 2019. jcs227850.
 - [9] Pierre de and Jacques Prost. *The Physics of Liquid Crystal*, volume 2. Oxford University Press, 01 1993.
 - [10] Denis Andrienko. Introduction to liquid crystals. *Journal of Molecular Liquids*, 267:520–541, 2018.
 - [11] Anne L Hitt, Alan R. Cross, and Robley Cook Williams. Microtubule solutions display nematic liquid crystalline structure. *The Journal of biological chemistry*, 265 3:1639–47, 1990.
 - [12] Edith Geigant, Karina Ladizhansky, and Alexander Mogilner. An integro-differential model for orientational distributions of f-actin in cells. *SIAM J. Appl. Math.*, 59:787–809, 1997.
 - [13] Igor S. Aranson and Lev S. Tsimring. Theory of self-assembly of microtubules and motors. *Phys. Rev. E*, 74:031915, Sep 2006.
 - [14] V Rühle, Falko Ziebert, R Peter, and Walter Zimmermann. Instabilities in a two-dimensional polar-filament-motor system. *The European physical journal. E, Soft matter*, 27:243–51, 11 2008.
 - [15] Shantia Yarahmadian and Masoud Yari. Phase transition analysis of the dynamic instability of microtubules. *Nonlinearity*, 27, 10 2013.
 - [16] P. M. Chaikin and T. C. Lubensky. *Mean-field theory*, page 144–212. Cambridge University Press, 1995.
 - [17] Shang-Keng Ma. *Modern theory of critical phenomena*. Routledge, 2018.
 - [18] Marileen Dogterom and Stanislas Leibler. Physical aspects of the growth and regulation of microtubule structures. *Phys. Rev. Lett.*, 70:1347–1350, Mar 1993.
 - [19] Adam R. Lamson, Jeffrey M. Moore, Fang Fang, Matthew A. Glaser, Michael J. Shelley, and Meredith D. Betterton. Comparison of explicit and mean-field models of cytoskeletal filaments with crosslinking motors. *The European Physical Journal E*, 44:1–22, 2021.
 - [20] Xia-qing Shi and Yu-qiang Ma. Understanding phase behavior of plant cell cortex microtubule organization. *Proceedings of the National Academy of Sciences*, 107(26):11709–11714, 2010.
 - [21] Vladimir A. Baulin, Carlos M. Marques, and Fabrice Thalmann. Collision induced spatial organization of microtubules. *Biophysical Chemistry*, 128(2):231–244, 2007.
 - [22] Rhoda J. Hawkins, Simon H. Tindemans, and Bela M. Mulder. Model for the orientational ordering of the plant microtubule cortical array. *Phys. Rev. E*, 82:011911, Jul 2010.
 - [23] N. M. Ferrers. *An Elementary Treatise on Spherical Harmonics and Subjects Connected with Them*. Macmillan and Co., London, 1877.
 - [24] Kendall Atkinson and Weimin Han. *Spherical Harmon-*

- ics and Approximations on the Unit Sphere: An Introduction*. Lecture Notes in Mathematics. Springer Berlin Heidelberg, Berlin, Heidelberg, 2012 edition, 2012.
- [25] V. Mirabet, P. Krupinski, O. Hamant, E. M. Meyerowitz, H. Jönsson, and A. Boudaoud. The self-organization of plant microtubules inside the cell volume yields their cortical localization, stable alignment, and sensitivity to external cues. *PLoS Comput Biol*, 14:e1006011, 2018.
- [26] Pauline Durand-Smet, Tamsin A. Spelman, Elliot M. Meyerowitz, and Henrik Jönsson. Cytoskeletal organization in isolated plant cells under geometry control. *Proceedings of the National Academy of Sciences*, 117(29):17399–17408, 2020.
- [27] Xavier Lamy. Uniaxial symmetry in nematic liquid crystals. *Annales de l'Institut Henri Poincaré C, Analyse non linéaire*, 32(5):1125–1144, 2015.
- [28] Hubert Kalf. On the expansion of a function in terms of spherical harmonics in arbitrary dimensions. *Bulletin of the Belgian Mathematical Society - Simon Stevin*, 2(4):361 – 380, 1995.
- [29] Ram Dixit and Richard Cyr. Encounters between Dynamic Cortical Microtubules Promote Ordering of the Cortical Array through Angle-Dependent Modifications of Microtubule Behavior[W]. *The Plant Cell*, 16(12):3274–3284, 12 2004.
- [30] Antonina Roll-Mecak and Francis J McNally. Microtubule-severing enzymes. *Current Opinion in Cell Biology*, 22(1):96–103, 2010. Cell structure and dynamics.